Acta Cryst. (1976). B32, 526

Modulated Structure of an Intermediate Plagioclase. II. Numerical Results and Discussion

BY KAREL TOMAN

Department of Geology, Wright State University, Dayton, Ohio, U.S.A.

AND A. J. FRUEH

Department of Geology and Institute of Materials Science, University of Connecticut, Storrs, Connecticut, U.S.A.

(*Received* 27 *December* 1974; *accepted* 1 *July* 1975)

With main reflections (*a*) and satellite reflections (*e* and *f*) from a plagioclase of composition An_{55}, least-squares refinements based upon the models discussed in the preceding paper were carried out. The crystal was found to consist of out-of-step domains, each containing additional faulting (modulation). The data are consistent with both centrosymmetric and non-centrosymmetric models. If a centrosymmetric model is accepted, the centrosymmetric domains are related by translation vectors having $c/2$ as their component. If non-centrosymmetric, the non-centrosymmetric domains are related to each other by inversion. Various details of the modulation structure were determined with a fair degree of reliability: the character of the Na/Ca environments in An_{55} plagioclase, their relationship to similar environments in anorthite and their change as related to modulation; also, the pattern of Si/Al substitution and its change due to modulation. The substitution pattern of the Na/Ca ions was determined with less reliability.

1. Introduction

Before discussion of the results of the numerical calculations based on the models introduced in the preceding paper (Toman & Frueh, 1976, henceforth referred to as TF6),* one fact which had a decisive effect on the selection of plausible models must be considered. It is well known that the intensity of satellite reflections in plagioclase is generally different for reflections belonging to the same satellite pair (reflections at $\mathbf{B}_H+\boldsymbol{\beta}^e$ and $\mathbf{B}_H-\boldsymbol{\beta}^e$, where $\mathbf{B}_H$ is a position vector of a *b* reflection and $\boldsymbol{\beta}^e$ is the separation of the *e* satellite from its closest *b* reflection). Because of Friedel's law, the intensity of a reflection at $\mathbf{B}_H-\boldsymbol{\beta}^e$ is equal to the intensity of a reflection at $\mathbf{B}_{\overline{H}}+\boldsymbol{\beta}^e$ and therefore different from the intensity of a reflection at $\mathbf{B}_H+\boldsymbol{\beta}^e$. If a Patterson map using satellite reflections of one kind only (for instance, reflections at $\mathbf{B}_H+\boldsymbol{\beta}^e$ where H is varied) is calculated, the result is a map in complex space, where the real part depends on terms such as $[J(\mathbf{B}_H+\boldsymbol{\beta}^e)+J(\mathbf{B}_{\overline{H}}+\boldsymbol{\beta}^e)]/2$, and the imaginary part depends on terms such as $[J(\mathbf{B}_H+\boldsymbol{\beta}^e)-J(\mathbf{B}_{\overline{H}}+\boldsymbol{\beta}^e)]/2$ (see TF4 for details). Peaks on real and imaginary maps have a very similar shape, size and distribution; this indicates, as demonstrated in TF4, that modulation waves involved in individual Patterson peaks have phase differences different from 0 or π. For the Na/Ca sites, the phase difference found in TF4 is $0{\cdot}28\pi$; similar values were found for other Patterson peaks. The presence of these phase differences leads directly to a general inequality of the intensities of reflections composing a satellite pair; obviously, phase relationships of the modulation waves must be carefully taken into consideration if a good agreement between calculated and observed intensities is to be obtained for a modulated-structure model.

It might be of interest to remember that other approaches are possible in order to achieve this inequality of intensities in a satellite pair. In TF2, a modulation of the unit-cell dimensions was considered as a possibility, but subsequent calculation showed that this did not give satisfactory agreement, even qualitatively.

In the preceding paper (TF6), it was shown that the best agreement in the least-squares treatment of the *a* reflections was obtained for a faulted structure (random faulting by translation or inversion, as well as periodic modulation) containing 26 independent half-atoms in a 7 Å subcell, with the apparent space group $C\overline{1}$. Unfortunately, this was not the first 'average' structure to be adopted in the study. Considerable effort was spent on working with an unfaulted (but modulated) structure in space group $C1$ (see TF5) before this fact became apparent. The models based on a faulted 'average' structure had been developed from the earlier models in $C1$. For this reason, these calculations (which lead to a fairly low R value) will be reported here briefly, in spite of the fact that the 'average' structure on which they were based is only partially correct.

The intensities of *a* reflections, *e* satellites and *f* satellites, obtained as described in TF1 and TF2, are used as the basis for all our present numerical computations. The chemical composition of the sample is close to An_{55}.

2. Models based on an unfaulted 'average' structure

The initial least-squares calculations were based on 'average' coordinates published in TF5, where the 'av-

* Throughout the present paper, the preceding papers of this study, Toman & Frueh (1971, 1972, 1973*a*, *b* and *c*) will be referred to as TF1, TF2, TF3, TF4 and TF5, respectively.

erage' structure is unfaulted and non-centrosymmetric. The input displacements of all atoms were taken into this calculation from TF4; it was assumed that the directions of displacements of all sites from 'average' positions were the same ([07$\bar{2}$]) with amplitudes and phases as given in Table 1 of TF4.

In the first trials, using the least-squares program for *e*-satellite reflections (TF6), all amplitudes of *f* components of the modulation waves were set to zero, and the modulation of the occupation of the Na/Ca sites was neglected. The only variables to be refined were 26 displacement vectors and 26 phases of the *e* components of the displacement modulation waves. After a number of runs, the *R* value for 542 *e*-satellite reflections and 112 variables dropped to 0·31. At this time, it was very important to determine whether this relatively high *R* value was caused by the crudeness of the description of the shape of the modulation waves (the modulation wave used was a simple cosine wave), or by some more basic deficiency. To solve this question, a method similar to the heavy-atom technique used in the structure analysis of perfect structures was used. The largest contribution to the structure factors was from the Na/Ca sites; this is not only because of the number of electrons involved, but also because of the amplitude of the displacements of these atoms from their average positions. (On Patterson maps based on *e*-satellite intensities, the only observable vectors are those between the Na/Ca sites and the remaining sites.) For this reason, as a first step all sites except the Na/Ca sites were neglected in calculating the phases of the structure factors. The three-dimensional Fourier map calculated by using observed amplitudes of the structure factors which were associated with the calculated phases (based on Na/Ca sites only) gave not only peaks at the Na/Ca sites but also at $T_1(0)$, $T_1(m)$, $T_2(m)$, $O_c(0)$ and $O_c(m)$ sites [for key to symbols labeling the sites, see Megaw (1956)]. Here, it is necessary to remember that the peaks in Fourier maps calculated from *e* satellites are not images of atoms but, as shown in TF3, transforms of the generalized atomic scattering factors, and they carry information about both the direction and the phase of the displacement modulation waves. The presence on the maps of these additional peaks, located in the correct positions and showing displacements and phases of the modulation waves similar to those obtained in the least-squares calculation above, was very encouraging, because it meant that the displacements and phases of the modulation waves of the Na/Ca sites used for the phasing of the structure factors were correct. The next step was to phase satellite structure factors, using the modulation waves of the $T_1(0)$, $T_1(m)$, $T_2(m)$, $O_c(0)$ and $O_c(m)$ sites. On corresponding Fourier maps, transforms of the generalized atomic scattering factors of the Na/Ca sites and the $O_A(0)$ sites were found in addition to those used for phasing. In the last step, the phasing was based on all 14 confirmed sites. On the maps, the transforms of all 26 atoms were found.

The basic soundness of our set of *e* modulation waves having been confirmed, our least-squares program for *f* satellites was used to calculate the displacement and phases of the *f* components of the displacement modulation waves. After some difficulties, it was possible to extract from a Patterson function based on *f*-satellite intensities a set of displacements and phases which led to an *R* value of 0·36 after refinement. The basic correctness of the computation was tested as before, using *f* displacement waves related to 25 independent atomic sites in order to phase the structure factors of the *f* satellites. On maps calculated using these phases and the measured amplitudes of the structure factors, the transform of the 26th atom [$O_A(0)$] appeared in the correct place in spite of the fact that it was excluded from the phasing. This was again considered as an indication of the basic correctness of our solution. In this case, a more detailed examination was not undertaken because the accuracy of determining the *f* components of the modulation waves is much lower than that of the *e* components. One reason for this is purely experimental: *f* satellites have a much lower intensity and a considerably larger width than *e* satellites. Another reason goes deeper: the larger width of *f* satellites means either that the *f* component of the modulation waves is coherent over a smaller range than that of the *e* component, or that it is disturbed by more irregularities. Both of these reasons imply that the representation of the modulation wave by one infinite cosine wave is better for *e* satellites, where reflections are very sharp, than for *f* satellites.

After determination of the preliminary parameters of the *f* modulation waves, our least-squares program was again used for *e* satellites, where as input the previous results relating to *e* and *f* displacement waves were used but only the parameters relating to the *e* components of the modulation waves were open to refinement. Parameters of the *f* waves were taken as a block of fixed constants. Now the *R* value was reduced to 0·28 (542 *e*-satellite reflections; 116 parameters). In this calculation, the modulation waves defined by the occupation of the Na/Ca sites were also determined. The results of these calculations served as input into calculations based on the model with faulting, the necessity of which was apparent by that time.

3. Models based on a faulted average structure

The calculations were performed with coordinates of the 'average' structure published in Table 1 of TF6. As has been shown in § 4 of TF6 (and also in the Appendix of the present paper), it is possible to construct two different models of an 'average' structure of a faulted plagioclase (centrosymmetric and non-centrosymmetric), both leading to the same expression for the structure factor. For this reason, it is not necessary at this stage to make any decisions about the symmetry of our model.

The first and most important problem when dealing

with our faulted models was one of the phase angle α, previously discussed in § 4 of TF6. This phase angle was introduced in addition to the phase angles of the individual modulation waves of the atomic sites, and it represents either the phase difference between identical modulation waves in domains of opposite chirality (non-centrosymmetric model) or else the phase difference of modulation waves related to atomic sites connected by an inversion center (in the centrosymmetric model). These phase differences are necessary in order to obtain different values of intensities for satellites at $\mathbf{B}_H+\boldsymbol{\beta}^e$ and $\mathbf{B}_H-\boldsymbol{\beta}^e$ in our computation.

In the first runs using our least-squares program for *e* satellite reflections, the *e* components of displacement waves as obtained for an unfaulted, non-centrosymmetric model (§ 2, this paper) were used as input; *f* components of modulation waves were neglected and, as coordinates of the 'average' structure, those obtained by the conventional least-squares refinement of the *a* reflections and half-atoms in apparent space group $C\bar{1}$ were taken (see TF6). The phase angle α was held constant at several values; the best *R* value was obtained for $\alpha=0{\cdot}25\pi$. This value was accepted and held constant in all subsequent runs (Fig. 1).

In these calculations, both the displacements and the occupations associated with *e* components of the modulation waves were permitted to vary. The final *R* value was 0·27 (542 *e* satellites; 112 variable parameters).

The next step was to refine the parameters of the *f* components of the displacement waves, using *f* satellites. Here, the same set of coordinates of the 'average' sites was used as in the previous case; the displacement vectors and phases of the *f* displacement waves were taken from the calculation described in § 2 of this paper; the *e* components were neglected, and α was taken to be $0{\cdot}25\pi$. After a few trials, *R* was 0·30 for 318 *f* satellites and 112 variable parameters.

In the next step, refinement of the *e* satellites was resumed. Here, input consisted of the parameters of the *e* and *f* components of the modulation waves obtained in the calculations described in this section. As before, only the parameters of the *e* components were permitted to vary; *f*-component parameters were taken as a block of fixed constants. The *R* value was now 0·24 (542 reflections; 112 parameters). The inclusion of parameters defining the *f* components of the modulation waves caused quite a significant drop of the *R* value without the number of parameters being increased (parameters of the *f* waves were determined from the *f*-satellite intensities and not refined in this run).

Concluding this step, parameters of both components of the modulation waves (*e* and *f*) were taken as input data into the least-squares program for the *a* reflections [based on equation (2) in TF6]. Input coordinates of the 'average' sites were those refined using equation (1) in TF6. Refinement proceeded with the isotropic temperature factors (one common for *A* sites, one common for *T* sites and one common for O sites). The final *R* value was 0·071 for 82 parameters (see TF6). The change in the coordinates was rather small, but in some cases it was of the order of magnitude of the differences between the half-atoms.

Now, the whole sequence of refinements was repeated with these new coordinates. In all cases, an improvement in the *R* value was observed. The *R* value for the *f* satellites (318 satellites; 112 parameters) dropped to 0·27. The *R* value for the *e* satellites (492 satellites; 112 parameters) dropped to 0·215. The final parameters of the *e* and *f* components of the modulation waves are listed in Table 1.*

Before proceeding to discuss these values and to compare the structure of plagioclase based on them with other structures of feldspars, it is well to consider the reliability of the procedure.

First, there is the question of scale. All three types of reflections (*a* reflections, *e* satellites and *f* satellites) were measured on the same crystal, using the same equipment and conditions, and therefore it is reasonable to assume that they are approximately on the same relative scale. This scale was converted into the absolute scale by refinement of the *a* reflections. A scale obtained in this way should apply to the *e* and *f*

* A list of observed and calculated structure factors of the *a* reflections, *e* satellites and *f* satellites is deposited with the British Library Lending Division as Supplementary Publication No. SUP 31251 (19 pp., 1 microfiche). Copies may be obtained through The Executive Secretary, International Union of Crystallography, 13 White Friars, Chester CH1 1NZ, England.

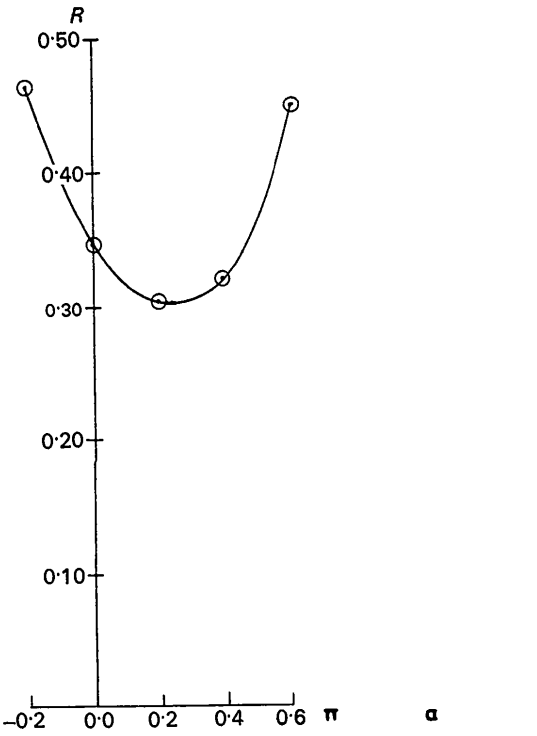

Fig. 1. Refinement of *e*-satellite reflections; the effect of phase angle α on the *R* value.

Table 1(*a*). *Fractional coordinates of sites in plagioclase subcell together with amplitudes and phases of e and f components of displacement modulation waves*

Coordinates of displacement vectors multiplied by 10^3; phases as fraction of 2π. Standard deviations in brackets.

Megaw symbol	No.	Coordinates x	y	z	e-Wave Δ_{1x}	Δ_{1y}	Δ_{1z}	$_{\Delta}\varphi_1$	f-Wave Δ_{2x}	Δ_{2y}	Δ_{2z}	$_{\Delta}\varphi_2$
$A(0000)$	$A1$	0·2688 (6)	−0·0239 (4)	0·0851 (8)	1 (1)	19 (1)	11 (1)	0·04	0 (1)	0 (1)	0 (1)	0·00
$A'(000c)$	$A1'$	0·2686 (6)	0·0290 (3)	0·0510 (7)	1 (1)	15 (1)	6 (1)	0·01 (2)	0 (1)	0 (1)	0 (1)	0·55 (10)
$T_1(000c)$	$T1$	0·0023 (7)	0·1676 (4)	0·1052 (8)	1 (1)	3 (1)	3 (1)	0·01 (3)	3 (1)	1 (1)	1 (1)	0·40 (2)
$T_1'(0000)$	$T1'$	0·0105 (7)	0·1626 (4)	0·1082 (8)	9 (1)	10 (1)	6 (1)	0·52 (2)	3 (1)	0 (1)	1 (1)	0·40 (2)
$T_1(m000)$	$T2$	0·0025 (7)	0·8171 (4)	0·1166 (8)	7 (1)	7 (1)	7 (1)	0·08 (3)	1 (1)	1 (1)	0 (1)	0·16 (4)
$T_1(m00c)$	$T2'$	0·0043 (7)	0·8190 (4)	0·1153 (8)	1 (1)	11 (1)	5 (1)	0·40 (2)	1 (1)	1 (1)	2 (1)	0·33 (2)
$T_2(0000)$	$T3$	0·6872 (7)	0·1099 (4)	0·1582 (8)	5 (1)	9 (1)	1 (1)	0·07 (2)	2 (1)	0 (1)	3 (1)	0·14 (2)
$T_2'(000c)$	$T3'$	0·6854 (7)	0·1095 (4)	0·1588 (8)	4 (1)	0 (1)	0 (1)	0·79 (8)	2 (1)	1 (1)	1 (1)	0·33 (4)
$T_2(m000)$	$T4$	0·6824 (7)	0·8797 (4)	0·1782 (8)	4 (1)	10 (1)	6 (1)	0·04 (2)	1 (1)	2 (1)	1 (1)	0·43 (3)
$T_2'(m00c)$	$T4'$	0·6825 (7)	0·8802 (4)	0·1787 (8)	3 (1)	1 (1)	8 (1)	0·57 (5)	2 (1)	1 (1)	0 (1)	0·01 (3)
$O_A(100c)$	$O1$	0·0079 (17)	0·1253 (10)	0·9887 (20)	9 (2)	13 (1)	4 (1)	0·44 (5)	5 (2)	0 (1)	3 (1)	0·31 (3)
$O_A'(2000)$	$O1'$	−0·0022 (17)	0·1318 (10)	0·9886 (21)	12 (3)	6 (1)	2 (1)	0·01 (4)	2 (2)	1 (1)	3 (1)	0·08 (2)
$O_A(2000)$	$O2$	0·5793 (17)	0·9942 (9)	0·1408 (21)	5 (2)	6 (2)	4 (1)	0·27 (4)	3 (2)	3 (1)	5 (1)	0·24 (2)
$O_A'(200c)$	$O2'$	0·5851 (17)	0·9924 (9)	0·1373 (20)	8 (2)	9 (1)	2 (1)	0·49 (3)	2 (2)	3 (1)	1 (1)	0·21 (2)
$O_B(000c)$	$O3$	0·8150 (17)	0·1024 (9)	0·0938 (20)	3 (2)	6 (1)	6 (1)	0·37 (4)	1 (2)	0 (1)	0 (1)	0·02 (2)
$O_B'(0000)$	$O3'$	0·8087 (18)	0·1111 (10)	0·0966 (20)	12 (3)	2 (1)	3 (2)	0·48 (4)	6 (2)	0 (1)	3 (1)	0·04 (12)
$O_B(m00c)$	$O4$	0·8113 (17)	0·8561 (9)	0·1177 (20)	4 (3)	4 (1)	14 (1)	0·46 (2)	6 (2)	1 (1)	0 (1)	0·20 (4)
$O_B'(m000)$	$O4'$	0·8260 (17)	0·8526 (10)	0·1305 (21)	8 (2)	5 (1)	7 (1)	0·07 (3)	2 (2)	0 (1)	1 (1)	0·16 (2)
$O_C(0zi0)$	$O5$	0·5145 (18)	0·7954 (9)	0·1361 (21)	5 (3)	18 (2)	9 (1)	0·52 (3)	3 (2)	2 (1)	1 (1)	0·18 (3)
$O_C'(0zic)$	$O5'$	0·5130 (17)	0·7938 (10)	0·1420 (20)	13 (3)	12 (1)	11 (1)	0·57 (3)	0 (2)	0 (1)	1 (1)	0·01 (6)
$O_C(mzi0)$	$O6$	0·5189 (18)	0·1884 (10)	0·1121 (20)	7 (3)	16 (1)	4 (1)	0·47 (2)	6 (2)	4 (1)	3 (1)	0·31 (2)
$O_C'(mzic)$	$O6'$	0·5135 (18)	0·1909 (9)	0·1053 (21)	12 (4)	7 (2)	2 (2)	0·33 (3)	3 (2)	3 (1)	4 (1)	0·12 (2)
$O_D(0000)$	$O7$	0·1907 (18)	0·1097 (9)	0·1962 (20)	5 (3)	8 (2)	1 (2)	0·28 (4)	2 (2)	0 (1)	2 (1)	0·12 (3)
$O_D'(000c)$	$O7'$	0·2076 (17)	0·1039 (9)	0·1890 (21)	10 (2)	13 (1)	1 (1)	0·47 (2)	2 (2)	0 (1)	2 (1)	0·50 (3)
$O_D(m000)$	$O8$	0·1943 (17)	0·8708 (9)	0·2110 (22)	5 (3)	10 (2)	5 (2)	0·08 (3)	1 (2)	3 (1)	3 (1)	0·35 (2)
$O_D'(m00c)$	$O8'$	0·1829 (17)	0·8642 (10)	0·2202 (20)	10 (2)	8 (1)	1 (1)	0·43 (4)	0 (2)	1 (1)	1 (2)	0·25 (5)

Table 1(*b*). *Coefficients and phases of occupation modulation waves (e and f components)*

Phases as fraction of 2π. Standard deviations in brackets.

Megaw symbol	No.	ε_{1J}	$_{\varepsilon}\varphi_{1J}$	ε_{2J}	$_{\varepsilon}\varphi_{2J}$
$A(000)$	$A1$	0·20 (2)	0·31 (5)	0·002 (2)	–
$A(00c)$	$A1'$	0·24 (2)	0·23 (4)	0·07 (2)	0·11 (5)

satellites as well, if the effective volume of the crystal contributing to the main reflections and to the satellites is the same. It seems obvious that the whole volume of the crystal (allowing for absorption) contributes to the *a* reflections; from the sharpness of the *e* satellites it also appears likely that the greater part of the volume of the crystal is ordered by *e* waves and contributes to the *e* satellites. But with the *f* satellites, only a smaller portion of the volume might be ordered by coherent *f* components of the modulation waves. In the calculation, it was assumed that the whole volume of the crystal contributes both to *a* reflections and to *e* satellites, and only half of the volume to *f* satellites. A direct scaling of the satellites is impossible because, in first-order approximation (especially for low 2θ angles), the satellite structure factors are proportional to the displacements.

Another question is the problem of convergence to the absolute minimum in our least-squares treatment. Several checks were made in order to obtain an empirical insight into this problem, including the following:

(i) After completing the refinement, the displacements of the modulation waves of the two atoms were interchanged to see if the refinement would return them to their original values. In a trial, shown in Fig. 2, atoms O6 and O6′ were affected. After 35 cycles the original conditions were well restored. In the same way, the $T1$ and $T1'$, O1 and O1′ and O3 and O3′ sites were tested.

(ii) The phases of the *e* occupation waves of the Na/Ca sites were interchanged and checked to see if they would return to their original values (Fig. 3).

(iii) For reasons to be discussed more fully in § 4, the phases of atoms $T1'$, $T2'$, $T3'$, $T4'$, O1′, O2′, O3′, O4′, O5′, O6′, O7′, and O8′ were shifted by π. The *R* value increased to 0·749; after 26 cycles, the displacements of some of the atoms changed sign, the phases of some of the other atoms changed by as much as $0{\cdot}5\pi$, and the *R* value decreased to 0·32, but did not improve further. The refinement had apparently slipped into a wrong minimum.

4. Discussion of the structure

The main purpose of this section is to show the relationships between the structures of feldspars as previously published, and the structure of intermediate plagioclase An_{55} as it can be compiled from 'average' coordinates of the atomic sites and from the parameters of the modulation waves (TF6 table, on deposit, and Table 1, present paper).

The comparison of the plagioclase superstructure with the structures of other feldspars is based upon analysis of the interatomic distances. Because the modulated structure continually changes character as it is examined point by point in the direction of the modulation wave vector, it is necessary to introduce 'local' interatomic distances in addition to the 'averaged' interatomic distances. Local interatomic distances change along the direction of the wave vector as a consequence of the modulation of the atomic sites. In the present work, the local interatomic distances are calculated at 16 equidistant points within the period of the e modulation wave (the wave vector of the e modulation wave is $B_T = -0{\cdot}062a^* - 0{\cdot}051b^* + 0{\cdot}219c^*$; a^*, b^*, c^*, are the edges of the reciprocal unit cell of anorthite). The term 'averaged interatomic distance' used here refers to the local interatomic distance, averaged over 16 points within the period of the superstructure; it differs slightly from the interatomic distance calculated from the coordinates of the 'average' structure. The unit-cell dimensions of our sample are $a = 8{\cdot}17$ (6), $b = 12{\cdot}86$ (2), $c = 14{\cdot}22$ (3) Å, $\alpha = 93{\cdot}6$ (2), $\beta = 116{\cdot}3$ (1) and $\gamma = 89{\cdot}8$ (1)°.

Table 2. *A–O distances in anorthite (A) and in bytownite (B) from Kempster, Megaw & Radoslovich* (1962) *and Fleet, Chandrasekhar & Megaw* (1966)

Megaw symbol	Distance to No.	X environment X_1	X_2	N environment N_1	N_2	Structure
$O_A(10)$	O1	2·62	2·47	2·48	2·46	*A*
		2·67	2·39	2·43	2·44	*B*
$O_B(2c)$	O2*	3·49	3·76	4	4	*A*
		3·53	3·96	–	–	*B*
$O_B(2c)$	O2**	4	3·74	3·38	3·24	*A*
		4·00	3·55	3·31	3·31	*B*
$O_B(mc)$	O4	3·84	3·25	2·49	2·50	*A*
		3·77	2·98	2·42	2·62	*B*
$O_C(00)$	O5	3·09	3·54	3·82	3·80	*A*
		3·05	3·61	3·83	3·68	*B*
$O_C(m0)$	O6	3·28	2·81	2·57	2·57	*A*
		3·30	2·70	2·50	2·61	*B*
$O_D(m0)$	O8	2·53	2·77	3·73	3·88	*A*
		2·57	3·10	3·84	3·70	*B*

(*a*) *Environment of the* Na/Ca *sites*

In their description of the structure of anorthite (Kempster, Megaw & Radoslovich, 1962) and of bytownite (Fleet, Chandrasekhar & Megaw, 1966), the various authors realized that the environments of the four independent Ca or Ca/Na ions are different. They distinguished between the sixfold-coordinated ions [$A(000)$ and $A(zi0)$] and the sevenfold-coordinated ions [$A(z00)$ and $A(0i0)$]; as can be seen from Table 2, which was compiled from their papers, the most striking difference between these two environments is in the interatomic distances. For instance, the distance to $O_B(m)$ is great in the sixfold and small in the sevenfold coordination; the opposite is true for the distance to $O_D(m)$.

To simplify the reference, the environment with interatomic distances similar to those of the sixfold coordination in the anorthite or bytownite environment is

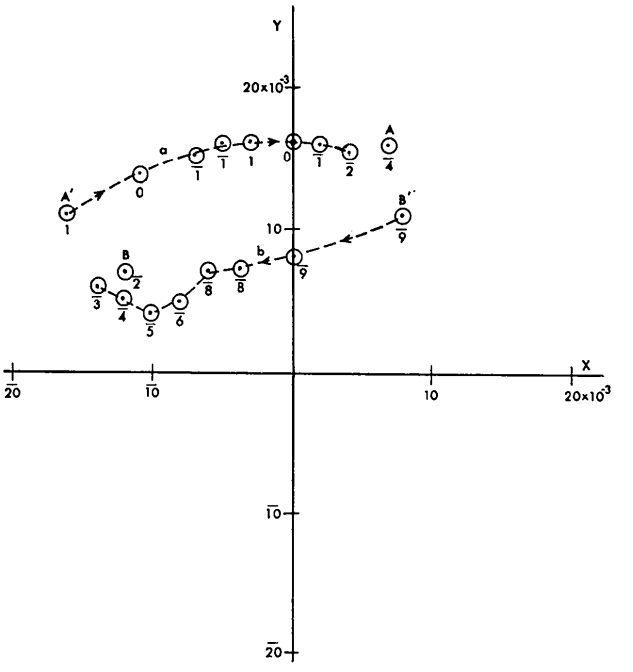

Fig. 2. Test of convergence. The displacement vectors of the modulation waves of atoms O6 and O6′ were moved from their final values to values described by points A' and B'. After 35 cycles they returned to close to their correct values, A and B. The numbers attached to the points are z coordinates in thousandths.

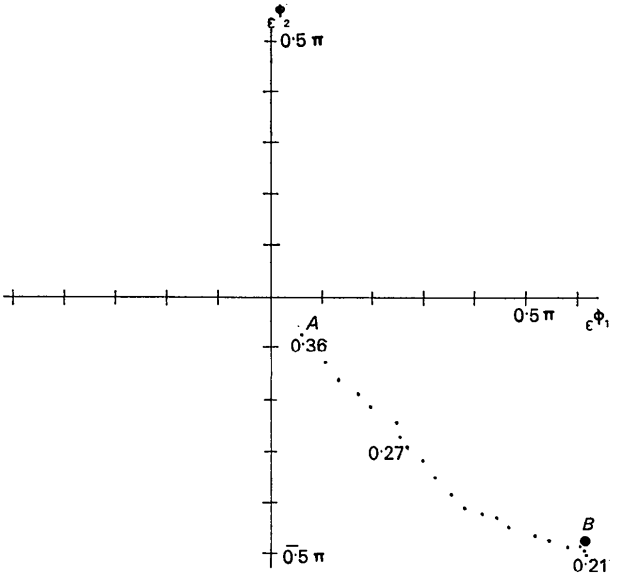

Fig. 3. Test of convergence. The phases of the occupation modulation waves of sites $A1$ and $A1'$ ($_\varepsilon\varphi_1$ and $_\varepsilon\varphi_2$) were changed from refined values to values described by point A. After 36 cycles they returned to close to their correct values (point B).

here called X; an environment with interatomic distances similar to those of the sevenfold coordination is called environment N. Furthermore, ions $A(000)$ and $A(zi0)$ are both in the X environment and yet their distances to the O atoms in anorthite are quite different. These differences are not accidental, because in bytownite the same trend can be seen. Therefore, the environment similar to the environment of ion $A(000)$ in anorthite or bytownite is here called environment X_1, and the environment similar to the environment of ions $A(zi0)$ is here called environment X_2. From Table 2 it can be seen that the distance to $O_B(mc)$ is greater in the X_1 environment than in the X_2 environment in both minerals; the opposite holds for the distance to $O_C(00)$. Similarly, an environment is here called an N_1 environment if the distances to O atoms are similar to those in the environment of the $A(z00)$ ion in anorthite or bytownite, and N_2 if the environment resembles the environment of the $A(0i0)$ ion.

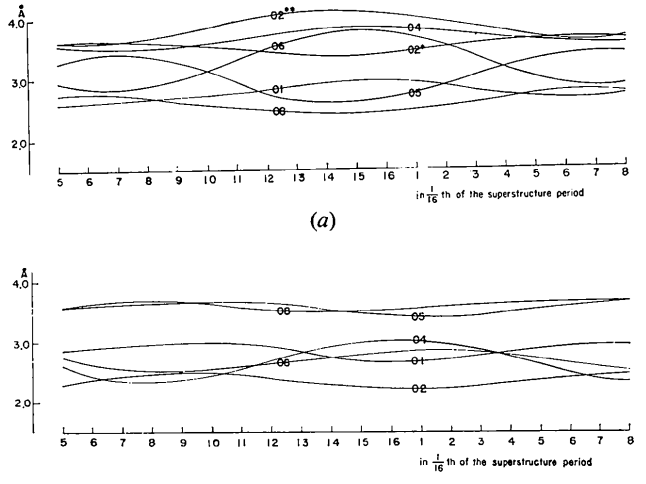

(*a*)

(*b*)

Fig. 4. Variation of the local A–O interatomic distances for the centrosymmetric case. (*a*) Calculated for site $A1$. (*b*) Calculated for site $A1'$.

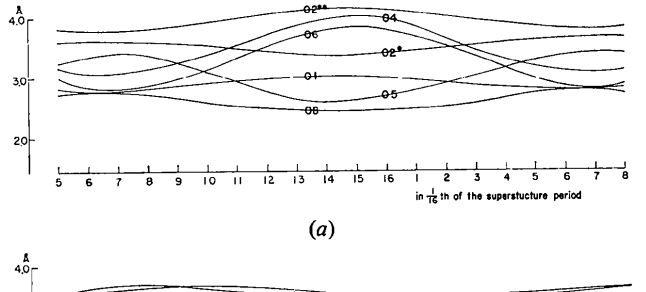

(*a*)

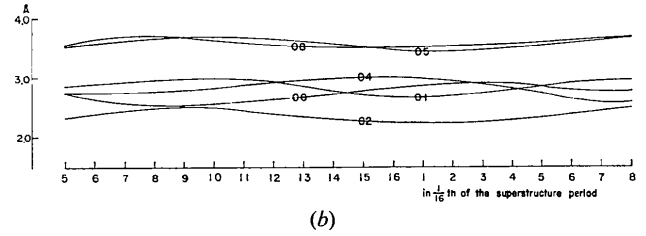

(*b*)

Fig. 5. Variation of the local A–O interatomic distances for the non-centrosymmetric case. (*a*) Calculated for site $A1$. (*b*) Calculated for site $A1'$.

As shown in the previous paper, our least-squares calculation covers two different cases, the non-centrosymmetric and the centrosymmetric. In our approximation, both cases give identical diffraction effects because of faulting. Therefore, no distinction based on least-squares results is possible; the consequence is that it is necessary to examine separately the interatomic distances corresponding to the non-centrosymmetric and centrosymmetric cases. At times the interatomic distances between closest neighbours are identical in both cases. The coordinates of the atomic sites in the ideal domains into which our faulted average structure is separated are reviewed in the Appendix.

Local interatomic distances calculated for the O atoms from Na/Ca site $A1$ and Na/Ca site $A1'$ are shown in Fig. 4(*a*) and (*b*) for the centrosymmetric case and in Fig. 5(*a*) and (*b*) for the non-centrosymmetric. The average coordinates of site $A1$ from which distances were calculated are 0·7688, 0·4761 and 0·0851, and for site $A1'$ they are 0·2314, 0·4710 and 0·4490 (derived from those listed in Table 1 by operations C and I, respectively – see Appendix).

As can be seen in Figs. 4(*a*) and (*b*) and 5(*a*) and (*b*), the variation of local distances caused by modulation is considerably larger for distances to ion $A1$ than to ion $A1'$. From Table 2 it can be seen that, in general, differences between crystallographically similar distances in X environments are larger than in N environments. For instance, the distance to oxygen $O_C(0)$ in anorthite is 3·09 Å in the X_1 environment and 3·54 Å in X_2 (a difference of 0·45Å), whereas in the N_1 environment it is 3·82 Å and in the N_2 environment it is 3·80 Å (a difference of 0·02 Å).

But this is not the only similarity between the environment of ion $A1$ and the X environments in anorthite, and between the environment of ion $A1'$ and the N environments in anorthite. If a comparison is made between Table 2 and Figs. 4 and 5, a much more striking parallel becomes evident. In all cases, if a particular distance shown in Table 2 is larger in the X_2 than in the X_1 environment, there is a maximum at the beginning of the range in Figs. 4(*a*) and 5(*a*). To mark the beginning of the range we will take a point where most interatomic distances are a maximum or minimum; in our case it is close to point 7 or 8. If, on the other hand, Table 2 shows a shorter distance in the X_2 than in the X_1 environment, we observe a minimum at the beginning of the range in Figs. 4(*a*) and 5(*a*). This can be seen more explicitly in Fig. 6(*a*).

The N environments shows similar characteristics; here the agreement is better in the case of the bytownite data. If there is a lower value for the N_1 than for N_2 environment shown in Table 2, a minimum is observable at the beginning of the range, and *vice versa*. For a summary, see Fig. 6(*b*).

These observations lead to the following conclusion: one feature of the plagioclase superstructure is the periodic change of the environment of the Na/Ca ions. The $A1$ ions, which are in the X environment, change periodically from the X_1 to the X_2 environment and back, with a period of $1/B_T$. The $A1'$ ions, which are in the N environment, change with the same period from N_1 to N_2 and back. Fig. 7(*a*) shows the Na/Ca environments at the beginning of the range, in the middle of the range and at the end of the range of the superstructure period for the centrosymmetric model; Fig. 7(*c*) shows the same for the non-centrosymmetric model; and Fig. 7(*b*) represents the environments of the Ca ions in anorthite.

It is important to realize that even if the centrosymmetric model is accepted, nowhere along the modulation wave is the structure exactly anorthite-like (even neglecting the occupations). In anorthite, X and N environments are related by the translation $\mathbf{c}/2$; in our model they are related by translation $(\mathbf{a}+\mathbf{b}+\mathbf{c})/2$ (assuming the centrosymmetric model). This means that the change of X_1 into X_2 and back, and the change of N_1 into N_2 and back is in phase in anorthite, but is shifted by phase angle π in our model. In order to be sure that this was really true, the least-squares refinement was recalculated, with all atoms involved in the N environments having their e modulation waves shifted by π (see § 3 of the present paper); the result was strongly negative.

(*b*) *Occupation of the* Na/Ca *sites*

Fig. 8 shows the variation of the atomic scattering factors within the period of the superstructure for both ion $A1$ and ion $A1'$, with their average coordinates as given in the previous section. The modulation of the atomic scattering factor is clearly apparent. The atomic scattering factor changes within the range expected for Na and Ca. The occupation modulation waves are not exactly in phase, nor are they exactly in phase with the variations of the environments discussed in the previous paragraph (Figs. 4 and 5). In order to be sure that the phases of the occupation modulation waves as obtained from the least-squares calculation (Table 1) corresponded to the lowest minimum of the residuals of the least-squares calculations, their values were changed considerably and the refinement was repeated (see § 3). After 30 cycles they returned to their previous values. It is difficult to tell if the phase difference of about $\pi/2$ as observed between the beginning of the range in Figs. 4 and 5 on one hand and the maxima positions in Fig. 8(*a*) on the other hand, is a computational anomaly or a genuine effect. The error in phase (the standard deviation as obtained from the least-squares calculation) is about $\frac{1}{16}$ of the range.

Fig. 8(*b*) and (*c*) shows the distribution of the Na and Ca ions in the plagioclase subcell at the beginning, in the middle and at the end of the range for the centrosymmetric and non-centrosymmetric cases, respectively. Because of the phase shift mentioned above, there is a phase shift of about $\frac{3}{16}$ of the period between Fig. 8 and Fig. 7. The error in a local value of the structure factor is about 0·3 of an electron.

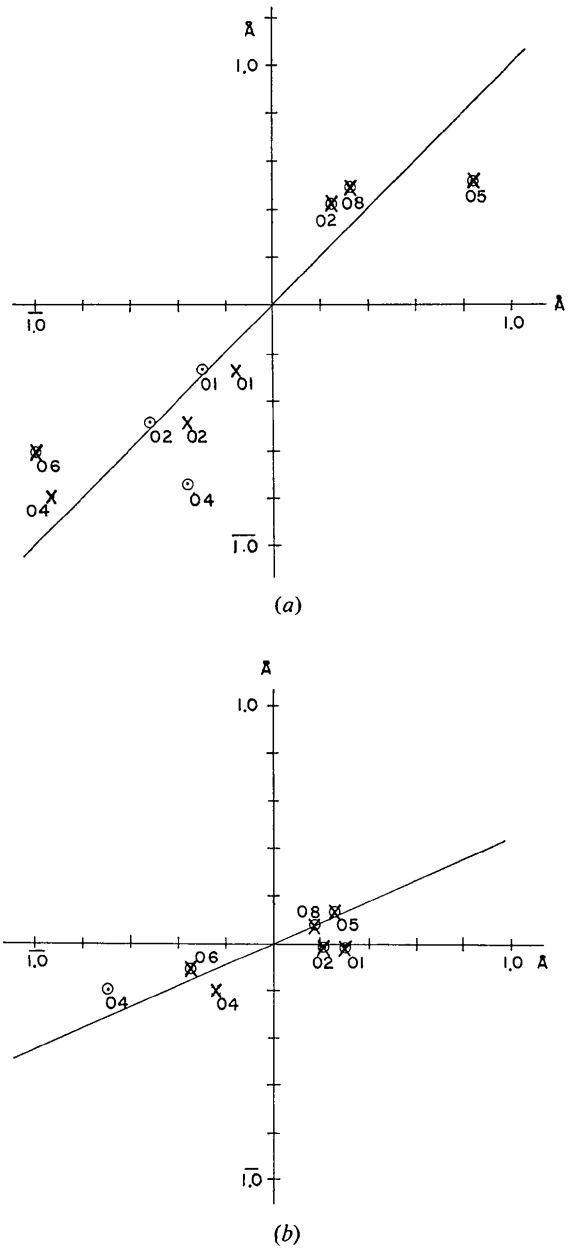

Fig. 6. Correlation between the A–O bond-length differences in bytownite and in the plagioclase superstructure. (*a*) Position $A1(zi0)$ in plagioclase. Horizontal axis: differences between A–O distances at the beginning and in the middle of the superstructure period. Centrosymmetric model ○, non-centrosymmetric model ×. Vertical axis: differences between the A–O distances in the X_2 and X_1 environments of bytownite. (*b*) Position $A1'(0ic)$ in plagioclase. Horizontal axis: differences between the A–O distances at the beginning and in the middle of the superstructure period. Centrosymmetric model ○, non-centrosymmetric ×. Vertical axis: differences between the A–O distances in the N_1 and N_2 environments of bytownite.

(*c*) *Occupation of the T sites*

The occupation of the *T* sites was not studied directly by evaluating the scattering factors of the *T* sites but, as usual, by using the interatomic distances between the *T* atoms and their four oxygen neighbours. As is well known (Ribbe & Gibbs, 1969), the average interatomic distance between the *T* atom and its four oxygen neighbours varies linearly from 1·605 Å for pure Si to 1·757 Å for pure Al in the *T* site of a feldspar.

The local interatomic distances between the *T* atoms and the O atoms in 16 equidistant points covering the whole period of the *e* modulation wave were calculated in the same way as was done for the *A*–O distances (see § 4(*a*), above). These local *T*–O distances were averaged over four *T*–O bonds originating at the same *T* atom, giving the 'average local *T*–O distances' shown for each independent *T* atom in Fig. 9. These average local *T*–O distances, taken together with the linear function mentioned above, permit calculation of the local contents of Al in each *T* site. Unfortunately, the accuracy of the results is not very great. From the standard deviations obtained in the least-squares calculation, it is possible to estimate the error in the 'average local *T*–O distance' as 0·02–0·03 Å, corresponding to 15–20% Al in local Al contents. Considerably more exact is the value which is obtained by averaging the 'average local *T*–O distances' over the superstructure period. This 'average *T*–O distance' has an error of only 0·01 Å, corresponding to 7% Al. The average *T*–O distances are shown in Table 3. In Table 4 the average coordinates are given for eight *T* atoms for which the average *T*–O distances are plotted in Fig. 9.

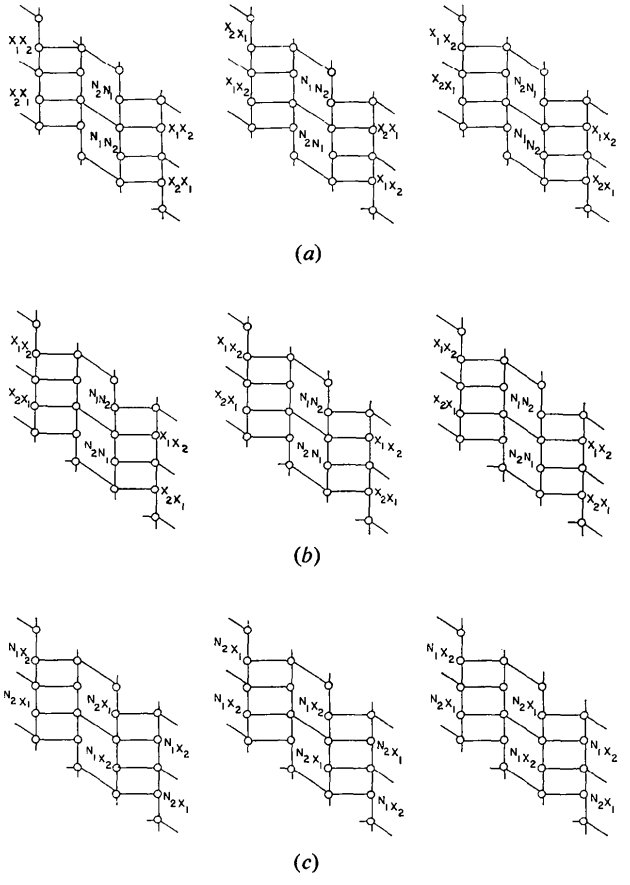

Fig. 7. Schematic pattern of one layer of *T* atoms in a 14 Å feldspar cell. Projection on (010), *a* edge vertical. (*a*) Arrangement of *X* and *N* environments in the centrosymmetric model of the plagioclase superstructure. Subcells at the beginning, in the middle and at the end of the superstructure period are shown. (*b*) Arrangement of the *X* and *N* environments in anorthite. (*c*) Arrangement of the *X* and *N* environments in non-centrosymmetric model of the plagioclase superstructure. Subcells at the beginning, in the middle and at the end of the superstructure period are shown.

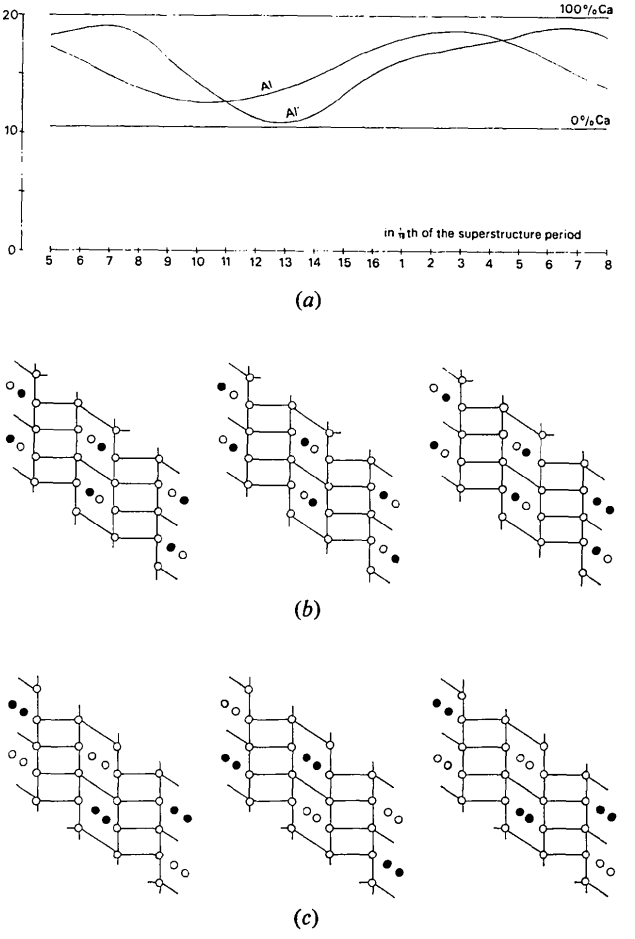

Fig. 8. Modulation of *A* site occupancies. (*a*) Local variation of the atomic scattering factor of the *A*1(*zi*0) and *A*1′(0*ic*) sites in the plagioclase superstructure. (*b*) Distribution of the Ca-rich and Ca-poor sites in the centrosymmetric model of the plagioclase superstructure – beginning, middle, end of the range. Ca-rich ●, Ca-poor ○. (*c*) Distribution of the Ca-rich and Ca-poor sites in the non-centrosymmetric model of the plagioclase superstructure – beginning, middle, end of the range. Ca-rich ●, Ca-poor ○.

Table 3. *Average T–O distances and corresponding average* Al *content of T sites*

Standard deviation of the distance, 0·01 Å; of the content, 7%.

	Average T–O distance	Al content		Average T–O distance	Al content
*T*1	1·70 Å	62%	*T*1′	1·70 Å	62%
*T*2	1·65	30	*T*2′	1·65	30
*T*3	1·64	25	*T*3′	1·65	30
*T*4	1·64	25	*T*4′	1·66	37

Table 4. *Fractional coordinates of T sites for which averaged local interatomic distances are shown in Fig.* 9 (*a*)–(*d*)

	x	*y*	*z*		*x*	*y*	*z*
*T*1	0·4977	0·3324	0·3948	*T*1′	0·0105	0·1682	0·1082
*T*2	0·5025	0·3171	0·1166	*T*2′	0·9957	0·1810	0·3847
*T*3	0·6872	0·1099	0·1582	*T*3′	0·8146	0·3905	0·3411
*T*4	0·1824	0·3797	0·1782	*T*4′	0·3175	0·1198	0·3213

It is obvious that the accuracy with which the 'average local *T*–O distances' are obtained does not justify any statement about the shape of the modulation wave. All that one can infer from Fig. 9 is the general trend of the Al distribution, especially the positions of maxima and minima. This, combined with our knowledge of the average Al contents as derived from the average *T*–O distances (Table 3), leads to a number of conclusions about the Al/Si distribution in plagioclase.

Following are two idealized interpretations of the curves shown in Fig. 9:

(i) We assume that the superstructure can be described in terms of the final configurations (at the beginning and in the middle of the superstructure period). The concentration of Al in the *T* sites of these final configurations can be determined if it is assumed that the volumes of the final configurations are equal. If, in Fig. 9, the curve gives an indication that for a given *T* site the Al content is zero on one of the two final configurations, then the Al content for the second final configuration is twice the corresponding average Al content of the site (Table 3). If, on the other hand, Fig. 9 indicates that for a given *T* site the Al content is 100% (when the corresponding curve approaches or exceeds the *T*–O value for pure Al) for one final configuration, then the same *T* site in the other final configuration has an Al content equal to the corresponding average Al content of the site minus 50%. If in Fig. 9 we have no clear indication of 0% or 100% Al in the *T* site of the final configurations, we estimate the Al content in both final configurations to be proportional to the values shown in Fig. 9, adjusting the percentages to match the average Al content in the site. Table 5 gives estimates of the Al content in each of the eight *T* sites in both final configurations (the beginning and the middle of the superstructure range). Centrosymmetric and non-centrosymmetric models present the same pattern [Fig. 10(*a*)]; Fig. 10(*b*) and (*c*) gives the distribution of the Al in a layer of *T* atoms in anorthite and in low albite. It is important to note that the modulations of the *A*–O distances (curves in Figs. 4 and 5) are very closely in phase with the modulation of the *T*–O distances (Fig. 9). This indicates that both features (the change in the Ca/Na environments and the occupation of the *T* sites) change simultaneously.

The relationship of the idealized Al distribution in our plagioclase sample [Fig. 10(*a*)] to the Al distribution in anorthite and in low albite [Fig. 10(*b*) and (*c*)] is apparent. In Fig. 10(*a*) a low concentration of Al is shown for sites which have no Al in anorthite and a high concentration of Al for sites which have pure Al both in anorthite and in low albite. On the remaining sites there is an intermediate concentration of Al.

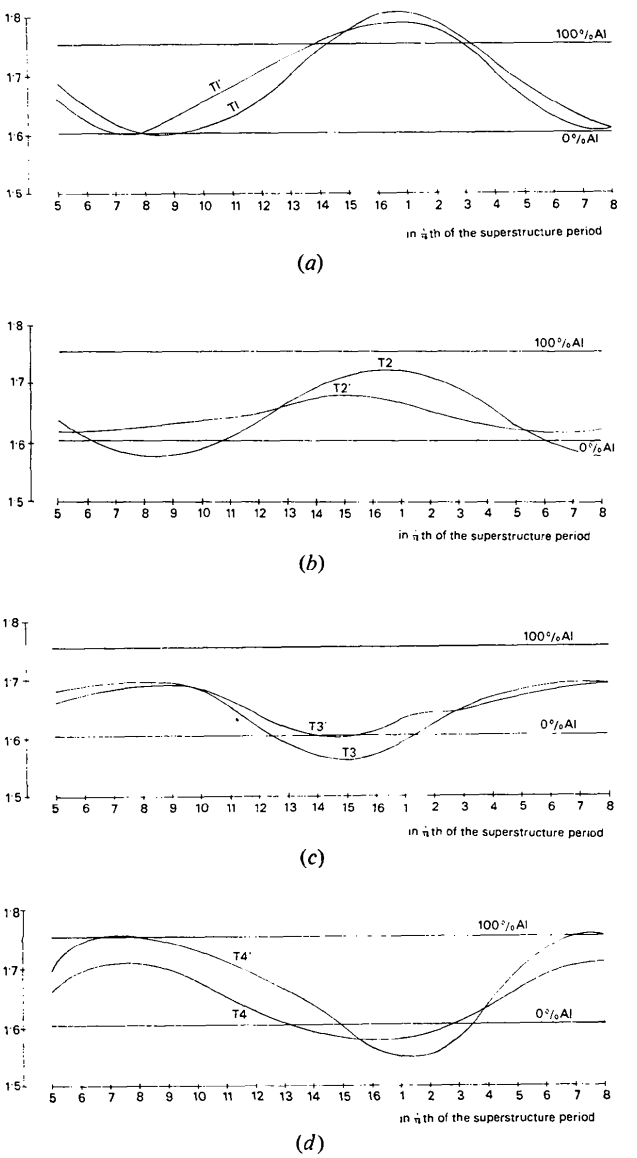

Fig. 9. Variation of the average local *T*–O distances in the plagioclase superstructure. (*a*) Sites *T*1 and *T*1′; (*b*) sites *T*2 and *T*2′; (*c*) sites *T*3 and *T*3′; (*d*) sites *T*4 and *T*4′.

Table 5. *Local* Al *content in T sites listed in Table* 4, *at the beginning and at the middle of the superstructure period*

Standard deviations, 15–20%.

	Local Al content			Local Al content	
	Beginning	Middle		Beginning	Middle
$T1$	20%	100%	$T1'$	20%	100%
$T2$	0	60	$T2'$	10	50
$T3$	50	0	$T3'$	60	0
$T4$	50	0	$T4'$	70	0

Fig. 10(*a*) shows only one layer of T atoms in plagioclase. The second layer can be derived easily by transforming sites by operation C (see Appendix) and changing the phase of the e modulation waves by π (interchanging the beginning of the range for middle of the range in Table 5 and *vice versa*).

(ii) Another idealized interpretation of the curves shown in Fig. 9 is shown in Fig. 12. These curves were derived as follows: any maximum or minimum on curves of the averaged local T–O distances (Fig. 9) is interpreted as 100% Al or 0% Al in the corresponding site. The widths of the ranges were adjusted to be in agreement with the average content of the sites (Table 3). No distinction was made between T and T' sites, and average Al contents were taken.

If these Si/Al distribution curves are applied, together with the usual requirement that sites related by translations $\mathbf{c}/2$ or $(\mathbf{a}+\mathbf{b})/2$ have modulation waves shifted in phase by π, a pattern is obtained in which anorthite-like regions alternate with albite-like regions twice in the superstructure period, and with no violation of the aluminum avoidance rule (Fig. 13). Obviously, Fig. 10(*a*) and Fig. 13 show the same structure but from different aspects. If Al contents are averaged by averaging over all unit cells at the beginning then in the middle part of the superstructure period, the occupations shown in Fig. 10(*a*) would result.

5. Conclusions

Following is a brief summary of the results of our study of the superstructure of plagioclase An_{55}:

(*a*) The average structure as obtained from the *a* reflections can best be described by using 26 independent half-atoms in a subcell with $c=7$ Å, in apparent space group $C\bar{1}$. The coordinates are shown in Table 1. This subcell can be split either into non-centrosymmetric cells or into centrosymmetric cells, as described in the Appendix.

(*b*) In intermediate plagioclase An_{55}, there are two

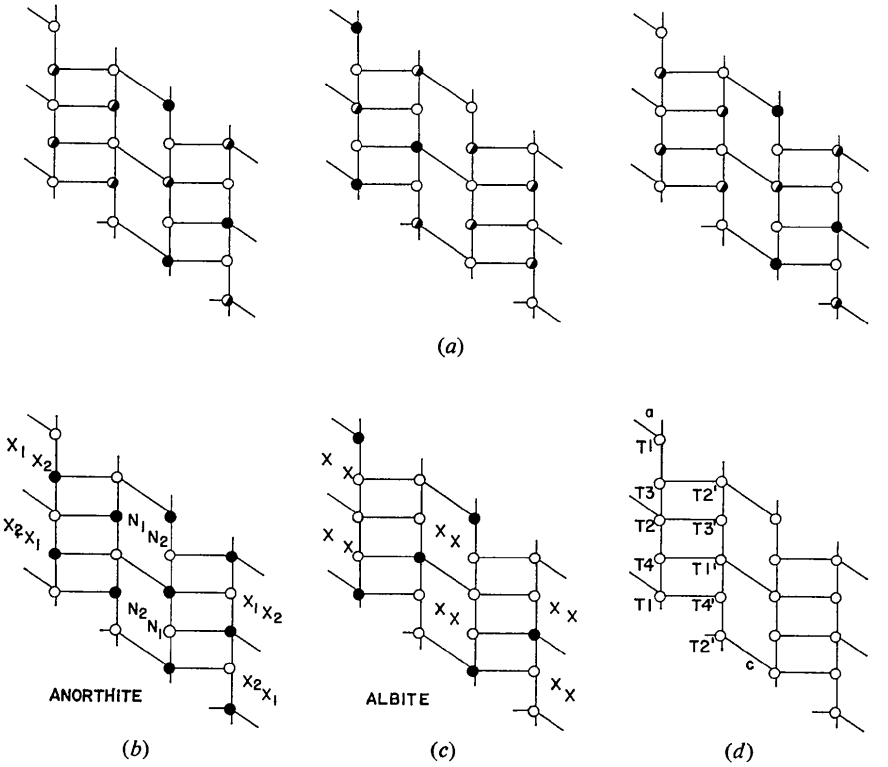

Fig. 10. Occupancies of the T sites. A site with an Al content above 75% ●; a site with an Al content between 25% and 75% ◒; a site with an Al content under 25% ○. (*a*) Plagioclase superstructure, beginning of the range, middle of the range, end of the range; (*b*) anorthite; (*c*) albite; (*d*) atomic positions and their symbols. Atoms in the second half of the subcell are derived from atoms in the first half by (i) inversion at the origin and translation by $(\mathbf{a}+\mathbf{b})/2$ (centrosymmetric case); or by (ii) translation by $\mathbf{c}/2$ (non-centrosymmetric case). In each case the e modulation wave changes phase by π. (Occupancy ● of sites $T1$ and $T1'$ changes into ○; similarly, occupancy ◒ of the remaining sites changes into ○, and *vice versa*.)

kinds of faulting: one is regular and periodic and is responsible for satellite reflections; the other is irregular and non-periodic and is responsible for the half-atom feature of the average structure.

(*c*) The crystal therefore consists of a number of domains (X-ray diffraction does not provide information about the shape of these domains), which can be centrosymmetric or non-centrosymmetric – a question as yet unresolved. If they are centrosymmetric, half of them must be 'out-of-step' by a translation containing as component **c**/2 with respect to the second half. If they are non-centrosymmetric, half of them must be in 'left-right' relationship to the second half of the domains. This irregular faulting leading to two types of domains is necessary in order to explain the half-atom feature of the average structure as calculated from the *a* reflections.

In addition to this irregular faulting leading to an irregular distribution of the domains, there is a regular and periodic faulting (modulation) inside the domains. This leads to satellite reflections.

(*d*) The most striking feature of the periodic faulting is the periodic inversion in the type of the Na/Ca environment, as described in § 4(*a*) [Fig. 7(*a*), (*b*), (*c*)].

(*e*) Another clearly established feature is the periodic change of pattern of the Al/Si occupancies. This change is in phase with the change in the environments of the *A* ions mentioned above [Fig. 11(*a*), (*b*)]. The Al/Si pattern shows a similarity to both albite and anorthite [see § 4(*c*)].

(*f*) This study also shows a modulation of the oc-

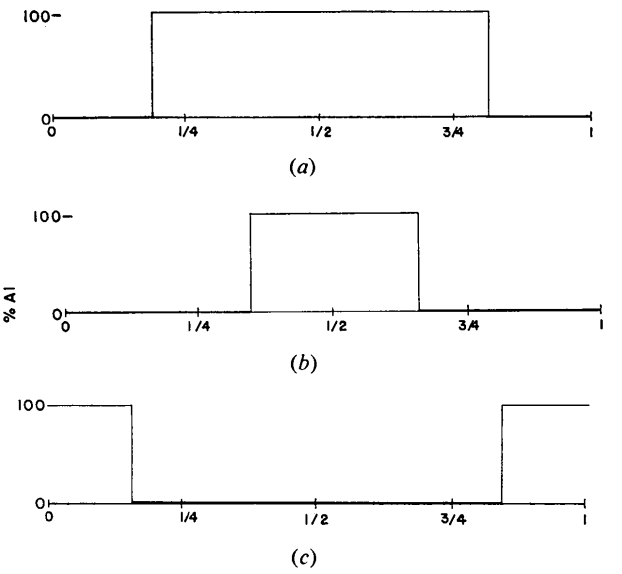

Fig. 12. Idealized Al, Si distribution in *T* sites. (*a*) *T*1(0000) sites; (*b*) *T*1(*mzi*0) sites; (*c*) *T*2(0000) and *T*2(*mzi*0) sites. The beginning of the range corresponds approximately to point 8-9 in Fig. **9.**

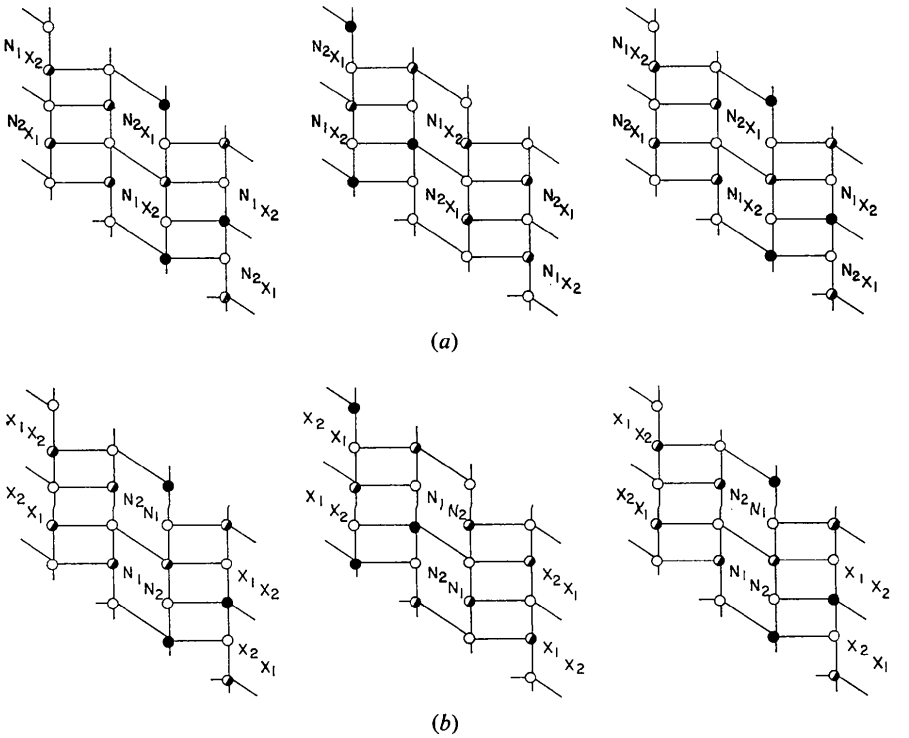

Fig. 11. Structure of the plagioclase superstructure showing both the twisting of the framework (changes in Na/Ca environment) and occupancies of the *T* sites. Beginning, middle and end of the superstructure period. (*a*) Non-centrosymmetric model, (*b*) centrosymmetric model.

cupancies of the *A* sites in a way predicted by Korekawa & Jagodzinski (1967); but this feature does not seem to be in phase with both features mentioned previously. Perhaps this may be connected with the easier mobility of the Na/Ca ions through the structure.

(*g*) It was not possible to establish any definite wave form; the simple cosine form of the modulation waves as used in the present study is only a mathematical approximation. For this reason, it is possible to describe only the final atomic configurations [Fig. 11(*a*), (*b*)] but not to tell anything about transitions between them.

(*h*) In view of this fact, it is necessary to accept (at least temporarily, until we know more about the wave form) the idea of a modulated structure of plagioclase consisting of parallel lamellae oriented perpendicular to the wave vector (0·062, 0·051, 0·219, with reference to the reciprocal cell of plagioclase). The thickness of the sandwich (both lamellae and the transitional zone) corresponds to the reciprocal value of the wave vector (63 Å). The ideal structure of each of them is given in Fig. 11(*a*) and (*b*) (assuming centrosymmetric or non-centrosymmetric symmetry); the structure labeled 'beginning of the superstructure period' in Fig. 11 corresponds to the first lamella, the structure labeled 'middle' corresponds to the second lamella, and the structure labeled 'end' corresponds to the beginning of a next sandwich of lamellae. As can be seen from Fig. 11(*a*) and (*b*), the relationship between the structures of both superstructure lamellae is a simple 'out-of-step' relationship with a translation by **c**/2 or by (**a**+**b**)/2 for the non-centrosymmetric case and by (**a**+**b**)/2 for the centrosymmetric case.

(*i*) The difference between the centrosymmetric and non-centrosymmetric cases is mainly in the way in which the Na/Ca environments are distributed. In the centrosymmetric type, the *X* and *N* types of environment are separated by translation **c**/2 (as in anorthite); in the non-centrosymmetric type, the *X* and *N* types of environment are placed on both sides of the points which are the centers of symmetry in anorthite. Except for the positions of the Na/Ca sites, there is only a slight difference in the coordinates of the atomic positions for both cases. No decisive evidence in favor of either case was obtained in the course of this study.

The support of this work by the National Science Foundation (GA 35246) is gratefully acknowledged.

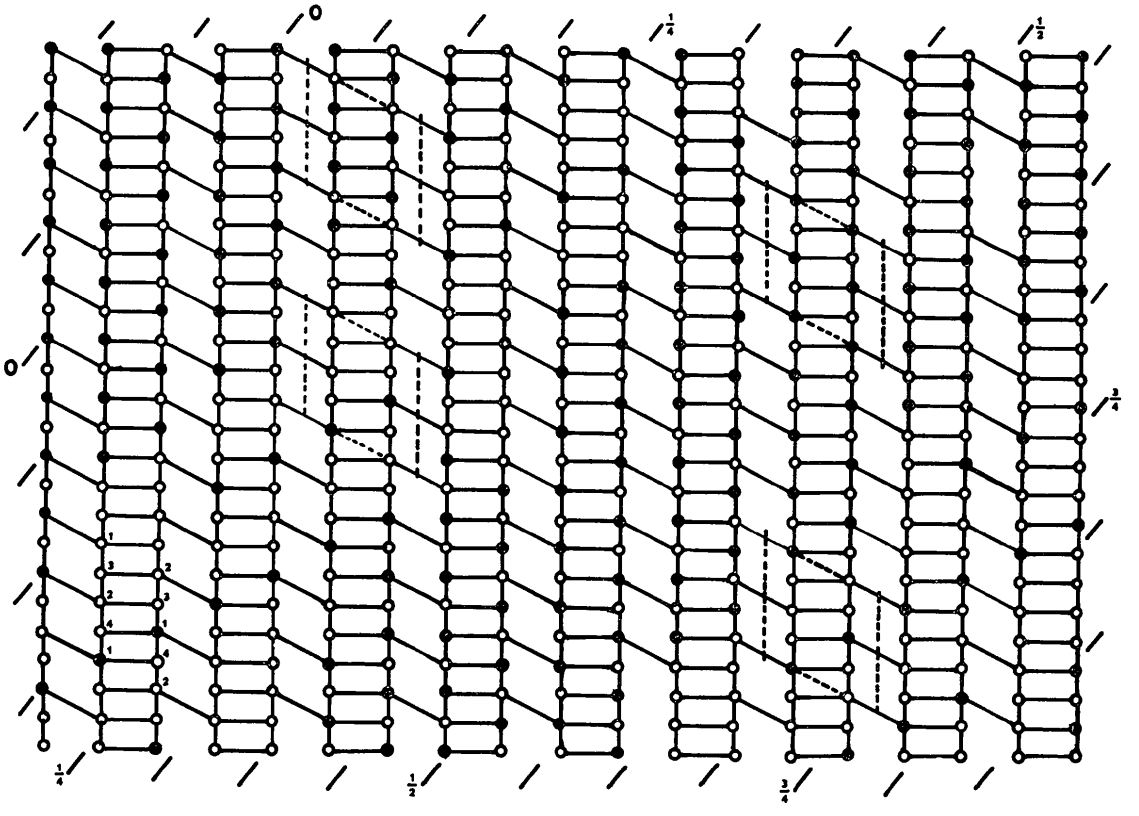

Fig. 13. Al (black circles), Si (open circles) distribution in a layer of *T* atoms as obtained from the idealized distribution curves in Fig. 12. Only part of the superstructure period is shown. Marks in the margin indicate the trace of the plane of the modulation wave with the plane of the layer, the numbers denoting the beginning (0), ¼, ½ and ¾ of the superstructure period. Dotted parallelograms indicate half-subcells with anorthite-like and albite-like arrangement. Numbers inside the figure denote the type of *T* site: 1 for the *T*1(0) site; 2 for the *T*1(*m*) site; 3 for the *T*2(0) site; and 4 for the *T*2(*m*) site.

APPENDIX

Our faulted average structure consisting of 26 independent half-atoms in the unit cell with $c=7$ Å, and in apparent space group $C\bar{1}$, can be split into two similar domains in two ways:

(1) *The non-centrosymmetric case*

The coordinates of 26 independent sites are as shown in Table 1. The presence of *e* satellites requires doubling of the *c* edge; therefore, an additional 26 sites are obtained by adding $\frac{1}{2}$ to the *z* coordinates of the initial set. Operation *C* [translation by $(\mathbf{a}+\mathbf{b})/2$] then creates an additional 52 sites, and the total is therefore 104 sites in a 14 Å unit cell. According to Korekawa & Jagodzinski (1967), the phases of the *e* modulation waves associated with the sites obtained by translation $\mathbf{c}/2$ or $(\mathbf{a}+\mathbf{b})/2$ are shifted by π compared with the phases of the modulation waves associated with the sites of the original set or with sites derived from the original set by a translation of $(\mathbf{a}+\mathbf{b}+\mathbf{c})/2$. Unit cells of this type constitute one set of domains; the other set of domains can be built up in the same way, but we start with coordinates from Table 1 inverted through the action of the inversion center at the origin. If these two domains have the same volume and if they diffract coherently, the average structure obtained from their common diffraction pattern will have the apparent symmetry $C\bar{1}$ and a period of $c=7$ Å (for the main *a* reflections).

(2) *The centrosymmetric case*

The coordinates of 13 independent sites (unprimed) are as shown in Table 1. To allow for the presence of *e* satellites (and in analogy with anorthite), the remaining primed sites in Table 1 are taken with the *z* coordinate increased by $\frac{1}{2}$ (a doubling of the *c* edge). The inversion center at the origin produces 26 additional related sites, and operation *C* gives an additional 52, with a total of 104 sites per unit cell, with $c=14$ Å. Unit cells of this type constitute one domain. Unit cells of the second domain are built up in the same way, but it is necessary to start with the primed coordinates in Table 1. The modulation waves of sites related to the original sites by translation $(\mathbf{a}+\mathbf{b})/2$ have phase difference π with respect to the modulation waves associated with sites of the original set. In addition to this, the modulation waves associated with all sites in the second domain have phase change π as compared with the corresponding modulation waves associated with the first domain. If these two sets of domains have the same volume and if they diffract coherently, the main *a* reflections will reveal an apparent $C\bar{1}$ symmetry and the period $c=7$ Å if the average structure is calculated from them.

References

FLEET, S. G., CHANDRASEKHAR, S. & MEGAW, H. D. (1966). *Acta Cryst.* **21**, 782–801.

KEMPSTER, C. J. E., MEGAW, H. D. & RADOSLOVICH, E. W. (1962). *Acta Cryst.* **15**, 1005–1035.

KOREKAWA, M. & JAGODZINSKI, H. (1967). *Schweiz. Miner. Petrogr. Mitt.* **47**, 269–278.

MEGAW, H. D. (1956). *Acta Cryst.* **9**, 56–60.

RIBBE, P. H. & GIBBS, G. V. (1969). *Amer. Min.* **54**, 85–94.

TOMAN, K. & FRUEH, A. J. (1971). *Acta Cryst.* B**27**, 2182–2186.

TOMAN, K. & FRUEH, A. J. (1972). *Acta Cryst.* B**28**, 1657–1662.

TOMAN, K. & FRUEH, A. J. (1973*a*). *Acta Cryst.* A**29**, 121–127.

TOMAN, K. & FRUEH, A. J. (1973*b*). *Acta Cryst.* A**29**, 127–133.

TOMAN, K. & FRUEH, A. J. (1973*c*). *Z. Kristallogr.* **138**, 337–342.

TOMAN, K. & FRUEH, A. J. (1976). *Acta Cryst.* B**32**, 521–525.